Chinese Chemical Letters 34 (2023) 108189

Contents lists available at ScienceDirect

Chinese Chemical Letters

journal homepage: www.elsevier.com/locate/cclet

Tailoring WB morphology enables d-band centers to be highly active for high-performance lithium-sulfur battery

Yuwei Zhao[a,1], Chang Liu[a,1], Chenyang Zha[a,b,1,*], Jing Li[b], Chongguang Lyu[a], Kaixi Wang[b], Junfeng Li[b], Kwan San Hui[c], Linghai Zhang[a,*], Kwun Nam Hui[b,*]

[a] Key Laboratory of Flexible Electronics (KLOFE), School of Flexible Electronics (Future Technologies), Institute of Advanced Materials (IAM), College of Materials Science and Engineering, Nanjing Tech University, Nanjing 211816, China
[b] Institute of Applied Physics and Materials Engineering (IAPME), Zhuhai UM Science & Technology Research Institute (ZUMRI), University of Macau, Taipa 999078, Macau SAR, China
[c] Engineering, Faculty of Science, University of East Anglia, Norwich NR4 7TJ, United Kingdom

ARTICLE INFO

Article history:
Received 3 December 2022
Revised 24 December 2022
Accepted 31 January 2023
Available online 3 February 2023

Keywords:
d-band centers
Tungsten borides
Electrocatalysis
Nanosheet
Lithium-sulfur battery

ABSTRACT

The d-band centers of catalysts have exhibited excellent performance in various reactions. Among them, the enhanced catalytic reaction is considered a crucial way to power dynamics and reduce the "shuttle" effect in polysulfide conversions of lithium-sulfur batteries. Here, we report two-dimensional-shaped tungsten borides (WB) nanosheets with d-band centers, where the d orbits of W atoms on the (001) facets show greatly promoting the electrocatalytic sulfur reduction reaction. As-prepared WB-based Li-S cells exhibit excellent electrochemical performance for Li-ion storage. Especially, it delivers superior capacities of 7.7 mAh/cm^2 under the 8.0 mg/cm^2 sulfur loading, which is far superior to most other electrode catalysts. This study provides insights into the d-band centers as a promising catalyst of two-dimensional boride materials

The high-performance lithium-sulfur (Li-S) battery is frequently regarded as one of the most promising devices for electric vehicles, and grid-scale energy storage systems, which have a large theoretical specific capacity (approximately 1600 mAh/g) [1–10]. Compared to commercial electrodes (140 and 170 mAh/g for $LiCoO_2$ and $LiFePO_4$, respectively), the sulfur cathodes show ten times better than that obtained for conventional positive electrode materials, which comes from the 16-electron conversion electrochemical processes ($S_8 + 16Li = 8Li_2S$) [11–14]. Moreover, sulfur material is naturally abundant (earth's crust is 0.03%−0.1%), environmentally friendly, and low costs (approximately 150 USD/ton) without toxicity [15]. However, the 16-electron-based solid-liquid-solid conversion process also causes sluggish kinetics of sulfur cathodes [17]. During the Li-S cell running, the sulfur cathodes generate polysulfide, and then the polysulfide escapes from the cathodes to dissolve in the electrolyte. Next, the migration of polysulfide moves to the lithium anode side to passivate the anode surface ("shuttle" effect) [18]. To address these shortages, these typically strategies show the use of functional materials to physically wrap and/or electrostatically anchor the polysulfides in the interior and surface of the electrode structure [1–5,18–22]. Nevertheless, the electrochemical processes of polysulfides are still unimproved, where the soluble polysulfides in electrolytes cause the insoluble final products on the anode, resulting in the exacerbation of the shuttling effect and rapid failure of Li-S batteries [8,23]. To further develop the performance of Li-S batteries [24], functional material using redox catalysis is used in batteries to overcome the shortcomings, where the enhanced electron and ion transport can boost the electrochemical reaction kinetics of polysulfides [11]. In addition, interface, defect, and size engineering are considered the effectual methods to enhance the performance of electrocatalysts [2,3,21,22], which can power the redox reactions of polysulfides by the ingenious design of materials. For instance, Duan team designed nitrogen and sulfur dual-doped graphene material to reduce the activation barrier [25], and enhance the redox kinetics of polysulfide conversion. In detail, the activated sites of catalysts anchor with polysulfides by the electron-rich Lewis bases of sulfur atoms, form the stabilizing transient states of adsorption, and promote the subsequent electrochemical reaction processes [25].

This means that creating activated sites is a promising approach to increasing the catalytic performance of catalysts [15]. Currently,

* Corresponding authors.
E-mail addresses: chenyangzha@um.edu.mo, iamcyzha@njtech.edu.cn (C. Zha), iam.lzhang@njtech.edu.cn (L. Zhang), bizhui@um.edu.mo (K.N. Hui).
[1] These authors contributed equally to this work.

https://doi.org/10.1016/j.cclet.2023.108189
1001-8417/

Zhang and co-workers reported the tailored band structure of catalysts to adjust the interaction between catalysts and polysulfides [26], where the electron affinities of 3d dopants can shift the d-band orbits of active sites, and further accelerate redox electron exchange for a fast electrochemical reaction [25,26]. Despite these encouraging progresses [15, 24-26], it can be inferred that the two-dimensional morphology of catalysts can expose abundant active sites on the surface [25], combined with the modification of the d-band orbits [26], which accelerates the multistep redox reaction of sulfur to build high-performance Li-S batteries under practical working conditions.

Herein, we report two-dimensional-shaped tungsten borides (WB) nanosheets with abundant tungsten atoms as polysulfides of catalysts sites by the effective d orbits, where unsaturation high valence states of d orbits offer the unsaturation 5d high valence states, several electron deficiencies in the redox electrochemical processes, and form the multiple coordination number from three to six which comes from the electron cloud changes by the losing or gaining electrons. Meanwhile, borophene subunits of WB represent the intrinsic conductivity as an efficient immobilizer and electrocatalyst to power electronic/ionic transport in the polysulfide conversion reaction. As a result, the synthesized WB-based Li-S cells exhibit a high area capacity (7 mAh/cm^2) under the 8.0 mg/cm^2, cycling stability, and stable Coulombic efficiency. The results reveal the connection between two-dimensional topography synthesis and catalytic center design as a structure-function strategy, which also offers a rational viewpoint to design d-band centers of boride in the catalytic field.

Fig. 1 presents an illustrated summary of d-band centers in Li-S chemistry. In the unmatched interface (Fig. 1a), the weak adsorption between metal sites (M) and polysulfides can cause the severe shuttle effect, resulting in poor cycle performance and rapid property fading of the battery [25,26]. Through the d-band tailoring strategy (Fig. 1b), the matched interface can offer the effective electrochemical conversion of polysulfides, which involves two electron transfers along with a complex configuration change of Li_2S_4/Li_2S_2 molecules. The suitable d-band orbits of metal atoms can further enhance the anchoring of polysulfides on the surface of the catalyst [25,26].

To further reveal the relationship between d-band orbits and catalytic action, the adsorption state is analyzed by the simulating density functional theory (DFT) [27–31]. The anions of sulfur atoms can interact with the cations of tungsten atoms, where the d-band orbits influence binding energies and catalytic conversion of polysulfides. More specifically, the polar molecule of Li_2S_4 with high soluble properties is considered the main candidate for polysulfides migration [32]. The WB (001) facets are taken as an adsorbed surface due to the two-dimensional morphology of the WB nanosheet. Next, the total orbits of WB are mainly composed of W atoms (5d orbits) and B atoms (2p orbits) in the density of states (DOS), and the total orbits of Li_2S_4 mainly come from 2p orbits of S atoms and 1s orbits of Li atoms (Fig. 2a). When Li_2S_4 is absorbed on WB (001) facet, the corresponding adsorption energy is −9.09 eV (Fig. 2c), where the strong adsorption of polysulfides can couple with the better performance of polysulfide conversion [32]. When Li_2S_4 adsorbs on the WB (001) surface (Li_2S_4-WB), the 5d orbits of W are overlapped with 2p orbits of S, which are around Fermi level (Fig. 2b). This implies that two terminal S atoms of Li_2S_4 are activated by the interfacial W atoms of WB, where the high electron density in the middle of catalyst-sulfur bonding can lower energy barrier of the conversion reaction [15,16,24]. Meanwhile, similar bonding shows in the 2p orbits of B and 1s orbits of Li.

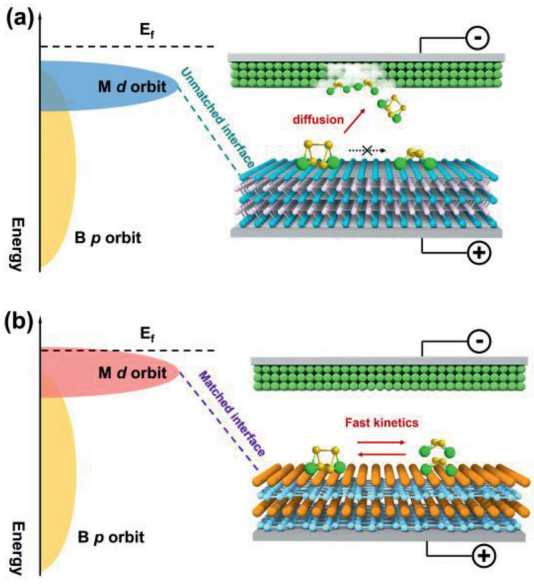

Fig. 1. Schematic illustrations of unmatched (a), and matched (b) d-band centers for the polysulfides of adsorption and catalysis.

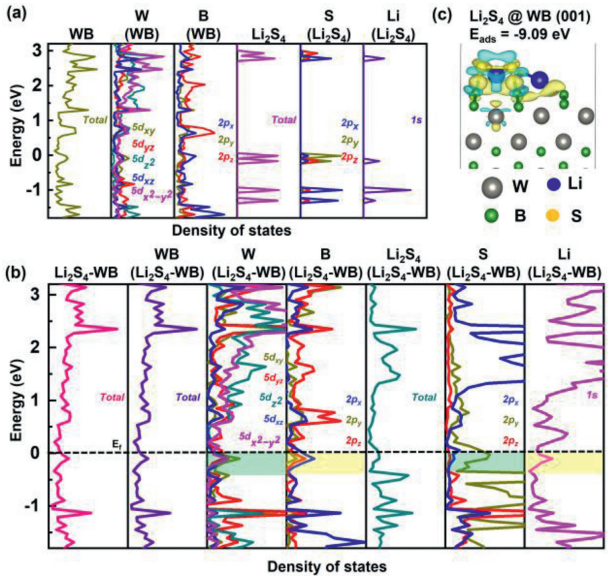

Fig. 2. (a) The DOS of pure WB and Li_2S_4. (b) The DOS and (c) binding energy value of Li_2S_4 adsorbed on the WB (001) surfaces.

The X-ray diffraction (XRD) pattern, and X-ray photoelectron spectroscopy (XPS) are applied to characterize the structure information of WB nanosheets. The XRD patterns (Fig. 3a) display sharp diffraction peaks in good agreement with standard tetragonal WB (space group, I41/amd, JCPDS No. 35–0738), which reveals the as-prepared WB material is a very stable crystal structure with good electronic conductivity [33]. Deconvolution of W 4f XPS spectrum ($4f_{7/2}$ and $4f_{5/2}$) shows W-O and W-B contributions (Fig. 3b), which is around 38–30 eV, respectively. The corresponding B 1s spectrum (Fig. 3c) is characteristic of the O-B (188 eV) and W-B (187 eV) in the WB material. Those result shows the surfaces of WB crystals have been spontaneously oxidized [34]. Importantly, scanning electron microscopy (SEM, Fig. 3d) and transmission electron microscopy (TEM, Figs. 3e and f, Fig. S1 in Supporting information) images reveal uniform morphology with a roughly sheet shape. A high-resolution TEM image (Fig. 3f) verifies that interlayer spacing (d) of WB is 0.3 nm, corresponding to the (101) diffraction planes. The selected area electron diffraction (SAED) pattern (inset of Fig. 3f) reveals diffraction dots of WB, suggesting

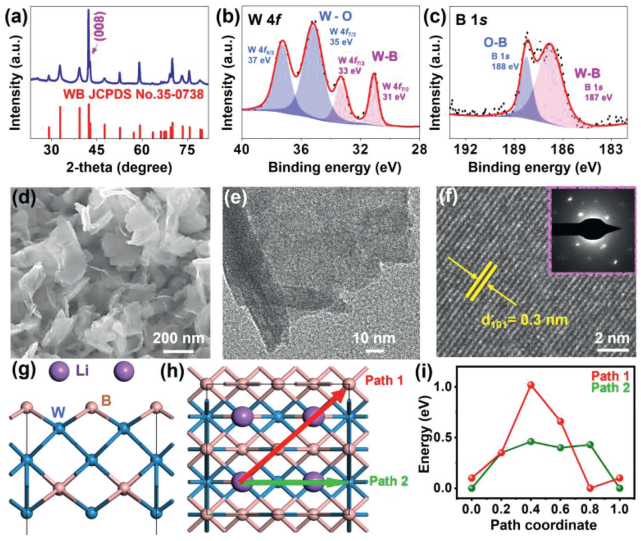

Fig. 3. (a) XRD pattern of WB. XPS spectra of (b) W 4f and (c) B 1s of WB. (d) SEM image, (e) HRTEM image, and (f) a high-magnification HRTEM image with an inset of SAED pattern of WB. (g) Simulated Li^+ ion diffusion on the WB. Schematic showing (h) the Path 1 and Path 2 diffusion path and (i) corresponding activation energy profile.

the single crystal structure indicates better electrical conductivity. The Li^+ ion mobility on the (001) facets of WB material is analyzed by the DFT (Fig. 3g), which is a key impact on the performance of the Li-S battery [27–29]. Path 1 represents the interface diffusion of Li^+ ions from W to B atomic sites, while Path 2 shows the interface diffusion of Li^+ ions from B to B atomic sites (Fig. 3h). The corresponding diffusion barriers are calculated to be 1.0 eV for Path 1 and 0.4 eV for Path 2 (Fig. 3i). Those features, combining the low diffusion barrier, afford 2D WB with better capability and stability during Li-S cell cycling [17,24].

Moreover, the liquid Li_2S_6 catholyte replaces the solid sulfur (S_8) in the WB-based Li-S cells, which is contributing to the electron/Li-ion transfer by the optimized contact areas. The high-resolution Li 1s XPS spectrum of pure Li_2S_6 exhibits a broad envelope of peaks, which are Li-S_B^0 (bridging sulfur), Li-S_T^- (terminal sulfur), and Li-S^{2-} (sulfide) bindings, respectively (Fig. 4a) [35–37]. The corresponding S 2p spectrum features a well-defined S $2p_{3/2}$ and S $2p_{1/2}$ doublet, suggesting the sulfite, S_B^0, S_T^- and S^{2-} bindings, respectively (Fig. 4b). Those results suggest that Li_2S_6 material has more chemical bonds, indicating that the better electrochemical activity enhances the polysulfide conversion reaction [32,36]. The SEM image of the electrode shows the uniform distribution between Li_2S_6 and WB (Fig. 4c and Fig. S2 in Supporting information). Next, the Raman spectra measurements of Li_2S_6 catholyte are performed as shown in Fig. 4d, which is around 398, 450, 510 and 537 cm^{-1}. The Raman spectra determine vibrational modes of Li_2S_6 molecules, which are attributed to radical anion S_6^{2-}. The Raman intensities (S_6^{2-}) indicates the symmetric S-S vibration belonging to the central S-S linkage of Li_2S_6 molecules, which shows chains with an even number of atoms [38]. The theoretical calculations of Li_2S_6 are also estimated for the electronic conductivity and chemical activity. The lowest unoccupied molecular orbital (LUMO) of Li_2S_6 and S_8 are −3.4 and −3.1 eV, and the highest occupied molecular orbital (HOMO) of Li_2S_6 and S_8 are −5.0 and −6.3 eV, respectively (Figs. 4e and f). The corresponding electronic band structure of Li_2S_6 has a 1.6 eV gap, which is much smaller than the intrinsic S_8 gap (3.2 eV) [32,36,39-41]. The difference in gap reveals the effective intrinsic redox carriers of Li_2S_6 are orders of magnitude more than that of S_8.

Furthermore, the cycling performances of 2D WB-based Li-S cells are investigated, and WB nanoparticles are acted as the comparison (3D WB). Those 2D and 3D WB-based Li-S cells (3.2 mA/cm^2) show the stabilized capacities of 720 and 440 mAh/g at 4.0 mg/cm^2 loading, retaining capacities of 620 and 380 mAh/g after 200 cycles with approximately 98% coulombic efficiency, respectively (Fig. 5a). The SEM images (Figs. S3a and b in Supporting information) show the morphology of 3D WB material is irregular particles, and the crystal structure (Fig. S3c in Supporting information) of 3D WB is the standard tetragonal WB (JCPDS No. 35–0738). The corresponding first discharge plateau (Fig. 5b) shows the S_8^{2-}/S_6^{2-} to S_4^{2-} in the long-chain polysulfide conversion (ΔC_1), the second discharge plateau is S_4^{2-} to S_2^{2-}/S^{2-} in the short-chain polysulfide conversion (ΔC_2), and the polarized voltage differences (ΔV) are measured at approximately 20% depth of discharge/charge [42–44]. In Fig. 5c, the ΔV of 2/3D WB-based Li-S cells present 0.40/0.40, 0.37/0.42, 0.41/0.46 and 0.40/0.45 V at the 50th, 100th, 150th and 200th cycles, respectively. The stabilized ΔV reveals the controllable polarization with the stable electrochemical reaction of polysulfide in the running 2D WB-based Li-S cell. Moreover, the $(\Delta C_2)/(\Delta C_1 + \Delta C_2)$ ratios of 2/3D WB-based Li-S cells reveal 65%/65%, 63%/63%, 66%/65% and 68%/66% after 50, 100, 150 and 200 cycles, respectively (Fig. 5d). Those corresponding ratios of $\Delta C_2/\Delta C_1$ of 2/3D WB-based Li-S cells are 1.8/1.8, 1.7/1.7, 1.9/1.9 and 2.1/1.9 after 50, 100, 150 and 200 cycles, respectively [42,45]. The conversion processes (S_8 to Li_2S_4 to Li_2S_2/Li_2S) indicate the high barrier of solid-state diffusion (solid S_8 to liquid Li_2S_4) with sluggish phase evolution, causing the electro-

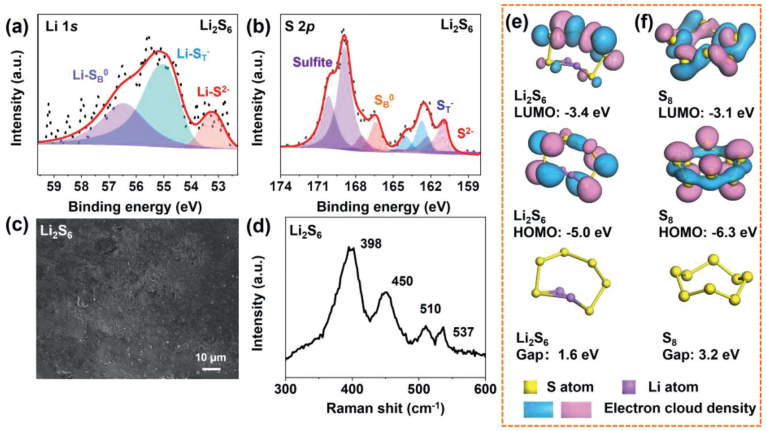

Fig. 4. Structural characterizations of Li_2S_6. XPS spectra of (a) Li 1s and (b) S 2p. (c) SEM image and (d) Raman spectrum. (e) The spatial charge density of the electronic states of HOMO and LUMO. (f) The spatial charge density of the S_8-based electronic states of HOMO and LUMO.

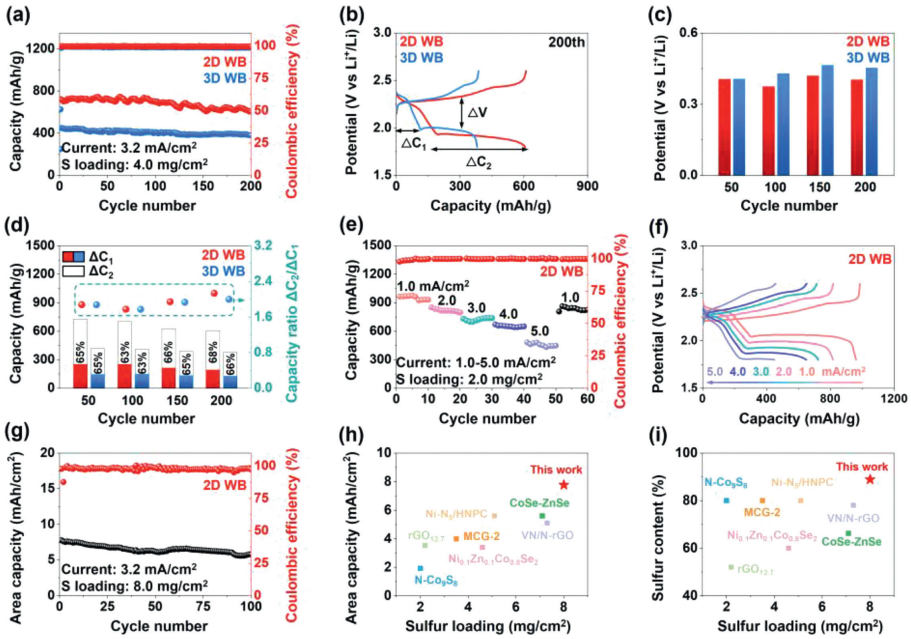

Fig. 5. (a) The cycling performance of 2D and 3D WB-based Li-S cells with (b) the corresponding charge and discharge profiles, (c) polarization voltages, (d) and ratio image of $\Delta C_2/\Delta C_1$. (e) Rate performances of cell from 1.0 mA/cm^2 to 5.0 mA/cm^2 with (f) the corresponding charge and discharge profiles. (g) The high area capacity of Li-S cell with high mass loading. (h) Comparison of areal capacity, and (i) content of sulfur of WB-based Li-S cell with other similar cathodes (detailed description of abbreviation in Table S1).

chemical reactions of polysulfides should be powered. The above-mentioned $\Delta C_2/\Delta C_1$ and $(\Delta C_2)/(\Delta C_1 + \Delta C_2)$ values show a slight difference in the different cycles, which indicates the enhanced electrochemical activity of polysulfide conversion [42,45,46]. With further rate performances at 1.0, 2.0, 3.0, 4.0 and 5.0 mA/cm^2, the WB-based cell shows reversible capacities of 970, 810, 700, 650 and 410 mAh/g, respectively (Fig. 5e). The corresponding discharge profiles have corresponded to S_8 to polysulfides and Li_2S_2/Li_2S, and the charge profiles are oxidation process from Li_2S_2/Li_2S to S_8 (Fig. 5f). For comparison, the 3D WB-based Li-S cell shows reversible capacities of 650, 470, 320, 120 and 90 mAh/g (Fig. S3d in Supporting information), respectively, which is the corresponding current at 1.0, 2.0, 3.0, 4.0 and 5.0 mA/cm^2. In what follows, the high sulfur loading (8.0 mg/cm^2) of WB cathode delivers superior capacities of 7.7 mAh/cm^2, retains 5.8 mAh/cm^2 after 100 cycles at 3.2 mA/cm^2 (Fig. 5g), where the performances of similar Li-S cells in the kinds of literature are summarized in Figs. 5h-i and Table S1 (Supporting information). Those WB-based Li_2S_6 cells show a better performance than other reported electrodes in the Li-S cells, and further reveal the efficient electrochemical kinetics of polysulfides. Furthermore, the electrochemical performance of 2D WB electrode is added in the electronic supplementary information (ESI), which is including CV curves (Figs. S4a-f in Supporting information) and the galvanostatic intermittent titration technique (GITT, Fig. S4g in Supporting information), and *in-situ* XPS spectra (Figs. S4h-k in Supporting information).

In summary, the 2D WB nanosheet catalyst has been designed by facile chemical synthesis, and the interfacial catalysis is revealed by theoretical calculations and the electrochemical method in the Li-S batteries. Benefiting from d-band centers of W sites, the 2D WB nanosheet shows an enhanced performance of Li-S cells compared to the intrinsic WB materials, which have an active interaction with the frontier orbitals of polysulfides. Meanwhile, the high performances of WB-based Li-S cells exhibit the better electrocatalytic activity of polysulfides and a greatly reduced reaction energy barrier with lower charge transfer resistance. Given the aforementioned features, the Li-S cells show significant improvements in capability and cycling stability with high sulfur loading. This work inspires an ingenious insight for interface engineering of 2D WB materials in the interacted phase transition-based multielectron redox reactions, but also provides an efficient interface engineering strategy of d-band centers catalysts at the atomic level.

Declaration of competing interest

The authors declare that they have no known competing financial interests or personal relationships that could have appeared to influence the work reported in this paper.

Acknowledgments

This work was supported by the National Natural Science Foundation of China (Nos. 61904080, 22205101), the Natural Science Foundation of Jiangsu Province (No. BK20190670), the Natural Science Foundation of Colleges and Universities in Jiangsu Province (No. 19KJB530008), the Macau Young Scholars Program (No. AM2020005), the High-Performance Computing Cluster (HPCC) of Information and Communication Technology Office (ICTO) at University of Macau, Science and Technology Development Fund, Macau SAR (Nos. 0191/2017/A3, 0041/2019/A1, 0046/2019/AFJ, 0021/2019/AIR), University of Macau (Nos. MYRG2017–00216-FST and MYRG2018–00192-IAPME), FDCT Funding Scheme for Postdoctoral Researchers (No. 0026/APD/2021), the Priority Academic Program Development of Jiangsu Higher Education Institutions (PAPD), the UEA funding, and Guangdong Basic and Applied Basic Research Foundation (No. 2022A1515110994).

Supplementary materials

Supplementary material associated with this article can be found, in the online version, at doi:10.1016/j.cclet.2023.108189.

References

[1] W. Lei, J. Xiao, H. Liu, Q. Jia, H. Zhang, Tungsten 2 (2020) 217–239.
[2] M. Du, P. Geng, C. Pei, et al., Angew. Chem. Int. Ed. 61 (2022) e202209350.
[3] X. Cao, M. Wang, Y. Li, et al., Adv. Sci. 9 (2022) 2204027.

[4] W. Li, X. Guo, P. Geng, et al., Adv. Mater. 33 (2021) 2105163.
[5] P. Geng, L. Wang, M. Du, et al., Adv. Mater. 34 (2022) 2107836.
[6] J.B. Goodenough, Energy Storage Mater. 1 (2015) 158–161.
[7] Y.V. Mikhaylik, J.R. Akridge, J. Electrochem. Soc. 151 (2004) A1969–A1976.
[8] C. Zha, S. Wang, C. Liu, et al., Energy Storage Mater. 47 (2022) 79–86.
[9] C. Zha, D. Wu, Y. Zhao, et al., J. Energy Chem. 52 (2021) 163–169.
[10] C. Zha, D. Wu, X. Gu, H. Chen, J. Energy Chem. 59 (2021) 599–607.
[11] A. Manthiram, Y. Fu, S. Chung, C. Zu, Y. Su, Chem. Rev. 114 (2014) 11751–11787.
[12] T. Zhang, L. Zhang, L. Zhao, X. Huang, Y. Hou, EnergyChem 2 (2020) 100036.
[13] Y. Li, X.T. Guo, S.T. Zhang, H. Pang, Rare Met. 40 (2021) 417–424.
[14] L. Du, H. Wang, M. Yang, L. Liu, Z. Niu, Small Struct. 1 (2020) 2000047.
[15] H. Ye, M. Li, T. Liu, Y. Li, J. Lu, ACS Energy Lett. 5 (2020) 2234–2245.
[16] J. Xiang, Y. Zhao, L. Wang, C. Zha, J. Mater. Chem. A 10 (2022) 10326–10341.
[17] H. Lin, S. Zhang, T. Zhang, et al., Adv. Energy Mater. 8 (2018) 1801868.
[18] P. Geng, M. Du, X. Guo, et al., Energy Environ. Mater. 5 (2022) 599–607.
[19] Y. Zhao, Z. Zhang, R. Wu, et al., Mater. Today Energy 21 (2021) 100793.
[20] Y. Zhao, J. Li, J. Xiang, et al., Mater. Today Energy 25 (2022) 100970.
[21] Y. Song, H. Gao, M. Wang, et al., EcoMat 4 (2022) e12182.
[22] B. Guan, X. Sun, Y. Zhang, et al., Chin. Chem. Lett. 32 (2021) 2249–2253.
[23] H. Ye, J. Sun, X.F. Lim, Y. Zhao, J.Y. Lee, Energy Storage Mater. 38 (2021) 338–343.
[24] H. Yuan, H.J. Peng, J.Q. Huang, Q. Zhang, Adv. Mater. Interfaces 6 (2019) 1802046.
[25] L. Peng, Z. Wei, C. Wan, et al., Nat. Catal. 3 (2020) 762–770.
[26] Z. Shen, X. Jin, J. Tian, et al., Nat. Catal. 5 (2022) 555–563.
[27] J.P. Perdew, K. Burke, M. Ernzerhof, Phys. Rev. Lett. 77 (1996) 3865.
[28] G. Kresse, J. Furthmüller, Phys. Rev. B 54 (1996) 11169.
[29] P.E. Blöchl, Phys. Rev. B 50 (1994) 17953.
[30] S. Grimme, J. Comput. Chem. 27 (2006) 1787–1799.
[31] G. Henkelman, H. Jónsson, J. Chem. Phys. 113 (2000) 9978–9985.
[32] G. Zhou, H. Tian, Y. Jin, et al., Proc. Natl. Acad. Sci. U. S. A. 114 (2017) 840–845.
[33] P.R. Jothi, K. Yubuta, B.P. Fokwa, Adv. Mater. 30 (2018) 1704181.
[34] J. Pan, C. Zhen, L. Wang, G. Liu, H. Cheng, Sci. Bull. 62 (2017) 114–118.
[35] I. Kartio, C. Basilio, R. Yoon, Langmuir 14 (1998) 5274–5278.
[36] Q. Pang, D. Kundu, M. Cuisinier, L. Nazar, Nat. Commun. 5 (2014) 1–8.
[37] F. Lindgren, C. Xu, J. Maibach, et al., J. Power Sources 301 (2016) 105–112.
[38] M. Hagen, P. Schiffels, M. Hammer, et al., J. Electrochem. Soc. 160 (2013) A1205.
[39] Y. Zhao, H. Yin, Z. Zhang, et al., Sustainable Energy Fuels 5 (2021) 3134–3142.
[40] C. Zha, F. Yang, J. Zhang, et al., J. Mater. Chem. A 6 (2018) 16574–16582.
[41] C. Zha, X. Gu, D. Wu, H. Chen, J. Mater. Chem. A 7 (2019) 6431–6438.
[42] H. Ye, J. Sun, S. Zhang, et al., ACS Nano 13 (2019) 14208–14216.
[43] T. Wu, J. Qi, M. Xu, D. Zhou, Z. Xiao, ACS Nano 14 (2020) 15011–15022.
[44] Y. Zhao, D. Wu, T. Tang, et al., J. Mater. Chem. A 10 (2022) 4015–4023.
[45] D. Gueon, J.T. Hwang, S.B. Yang, et al., ACS Nano 12 (2018) 226–233.
[46] H. Al Salem, G. Babu, C.V. R.ao, L.M.R. Arava, J. Am. Chem. Soc. 137 (2015) 11542–11545.